ELSEVIER

International Journal of Solids and Structures 41 (2004) 3607–3624

INTERNATIONAL JOURNAL OF SOLIDS and STRUCTURES

www.elsevier.com/locate/ijsolstr

Finite element formulation for finite deformation, isotropic viscoplasticity theory based on overstress (FVBO)

S. Gomaa [1], T.-L. Sham, E. Krempl *

Mechanics of Materials Laboratory, Rensselaer Polytechnic Institute, Troy, NY 12180-3590, USA

Received 20 May 2003; received in revised form 12 November 2003
Available online 11 March 2004

Abstract

The isotropic, unified state variable theory based on overstress consisting of a flow law and two tensor-valued and two scalar-valued stress-like state variables is extended to finite deformation. To this end the Cauchy stress rate and the rates of the two tensor-valued state variables are interpreted as Eulerian tensors. Their objective rates are based on the recently proposed logarithmic spin [Acta Mech. 124 (1997) 89] and on the fact that the logarithmic integration of the rate of deformation tensor results in the Hencky strain [Acta Mech. 124 (1997) 89]. The rate of deformation is equal to the sum of the elastic (the rate form of Hooke's law) and the inelastic rate of deformation, which depends on the overstress. Computational procedures are derived for the one-step forward gradient and the backward Euler methods. Numerical experiments show that no oscillations are observed in simple shear and that the integration of the elastic rate of deformation exhibits proper elastic behavior. Other numerical experiments show nonlinear rate sensitivity and the absence of strain rate history effects.

Keywords: Viscoplasticity; Finite deformation; Unified state variable theory; Overstress; Eulerian formulation

1. Introduction

Xiao et al. (1997) have recently introduced an objective logarithmic co-rotational rate, referred to as the logarithmic rate in the sequel. Using this logarithmic rate they have demonstrated that the logarithmic rate of the Hencky strain $\ln\mathbf{V}$ is exactly the rate of deformation tensor. They have further shown that the Hencky strain is the only strain tensor that has this property. These observations suggest the possibility of formulating a state variable theory on the basis of an Eulerian description and the logarithmic rates. These ideas are adopted in the present work to develop an isotropic, finite deformation viscoplasticity theory based on overstress (FVBO). This constitutive model has been implemented in ABAQUS; and among others, it has been used to simulate simple shear, free-end torsion and strain rate change tests. A hypoelastic

* Corresponding author. Tel.: +1-518-276-6985.
E-mail address: krempe@rpi.edu (E. Krempl).
[1] Present address: DePuy Orthopaedics, Inc., Warsaw, IN.

0020-7683/$ - see front matter © 2004 Elsevier Ltd. All rights reserved.
doi:10.1016/j.ijsolstr.2004.01.016

formulation employs the logarithmic stress rate. The inelastic rate of deformation is a function of the overstress, the difference between the stress and the equilibrium stress, which is a state variable of the theory. Repositories for isotropic and kinematic hardening are provided. Numerical experiments that have been conducted include:

(1) The calculation of the energy expended around a closed cycle with zero inelastic rate of deformation. No dissipation is found.
(2) Calculation of the responses in simple shear. No oscillations of the stress–strain curves are found.
(3) Calculation of the response for free-end torsion, the Swift Effect. The computed responses compare well qualitatively and quantitatively with experiments for monotonic loading. For loading and unloading the correspondence is not as good due to the isotropic nature of the FVBO.
(4) By comparing the responses to the same loading conditions for the Jaumann rate, the beneficial effects of the logarithmic rate become apparent.

In this work a basic theory for a finite deformation, isotropic Eulerian approach is introduced. Such a framework is used as a basis for developing a finite deformation viscoplasticity theory based on overstress, FVBO. It is well known that viscoplastic constitutive models are difficult to integrate numerically due to their stiffness. Two methods are presented: (i) a one-step forward gradient approximation, (Peirce et al., 1984), and (ii) an unconditonally stable implicit integration scheme based on the backward Euler method. The updated Lagrangian formulation is adopted in the formulation of the kinematics.

2. Constitutive model

The constitutive model is formulated in rate form using the Eulerian tensors Cauchy stress, $\boldsymbol{\sigma}$, and the rate of deformation, $\mathbf{D}$; and their deviators $\mathbf{s}$ and $\mathbf{d}^{\text{in}}$, respectively. It is generalized from the small strain version by introducing the rate of deformation and objective derivatives of the stress and all stress like state variables. The objective derivative chosen here is the co-rotational, logarithmic derivative introduced by Xiao et al. (1997). It will be shown below that the logarithmic rate and the logarithmic derivative have desirable properties. As in the small strain model the total rate of deformation can be viewed as the sum of the elastic and of the inelastic parts. This is not a kinematic statement, but a constitutive postulate on the rate of deformation.

The inelastic deformation rate depends on the overstress, the difference between the stress and the equilibrium stress deviators, $\mathbf{o} = \mathbf{s} - \mathbf{g}$. An overstress invariant or equivalent overstress $\Gamma = \sqrt{\frac{3}{2}\mathbf{o} : \mathbf{o}}$ is introduced, which is useful as is the unit tensor $\mathbf{n} = \sqrt{\frac{3}{2}}\frac{\mathbf{o}}{\Gamma}$, which points in the direction of the inelastic rate of deformation. The extension of the small strain theory (Krempl, 1996) leads to the elastic and the inelastic contribution as

$$\mathbf{D}^{\text{e}} = \mathscr{L}^{-1} : \hat{\boldsymbol{\sigma}}^{\log} \tag{1}$$

and

$$\mathbf{D}^{\text{in}} = \frac{3}{2}\overline{D}^{\text{in}}\frac{\mathbf{s}-\mathbf{g}}{\Gamma} = \sqrt{\frac{3}{2}}\overline{D}^{\text{in}}\mathbf{n} \tag{2}$$

It is readily seen that Eq. (2) is deviatoric.

The total rate of deformation is given by adding Eqs. (1) and (2)

$$\mathbf{D} = (\mathscr{L}^{-1} : \hat{\boldsymbol{\sigma}}^{\log}) + \sqrt{\frac{3}{2}}\overline{D}^{\text{in}}\mathbf{n} \tag{3}$$

In the above the quantity $\mathscr{L}^{-1}$ is the elastic, isotropic compliance tensor and $\overline{D}^{\text{in}} = \frac{\Gamma}{Ek[\Gamma]}$ is the effective inelastic strain rate from which the inelastic path length can be obtained by integration $\bar{e}^{\text{in}}[t] = \int^t \overline{D}^{\text{in}}[\tau]\,\mathrm{d}\tau$. The viscosity function $k[\Gamma]$ is a positive, decreasing function of Γ and controls the rate sensitivity, i.e. the spacing of the stress–strain diagrams at different loading rates when plastic flow is fully developed.

The logarithmic rate of any symmetric Eulerian tensor $\mathbf{G}$ is defined as

$$\widehat{\mathbf{G}}^{\log} = \dot{\mathbf{G}} + \mathbf{G}\boldsymbol{\Omega}^{\log} - \boldsymbol{\Omega}^{\log}\mathbf{G} \tag{4}$$

where a superposed dot denotes the material derivative, and $\boldsymbol{\Omega}^{\log}$ is the logarithmic spin that can be explicitly calculated by algebraic expressions, see Eqs. (42)–(49) of Xiao et al. (1997). The calculation is in terms of $\mathbf{W}$, the skew spin tensor, the rate of deformation tensor $\mathbf{D}$, and the left Cauchy–Green tensor $\mathbf{B}$.

It is important to note that the isotropic FVBO law does not require a separate stress or strain-space formulation. Referring to Eq. (3), it is seen that the second term of the right-hand side depends only on the present stress deviator and the equilibrium stress deviator (a possible dependence on the drag stress is not implemented in the flow law Eq. (3)). No strain measure is used in the formulation. The left-hand side and the first term on the right hand sides are rate terms. A fixed increment of $\mathbf{D}$ or $\hat{\boldsymbol{\sigma}}^{\log}$ is used in the first step to calculate the stress or strain increment. (To complete the formulation, the growth laws of the state variables are necessary and will be introduced later in this paper.) At the end of the incremental step the total stress (total strain) are known and become the initial conditions for the subsequent step. The solution is then established by many increments.

For the solution of boundary value problems the incremental time stepping is performed for a finite element integration point. Finite element procedures then augment this to solve actual boundary value problems.

For later use the inverted form of Eq. (3) is derived as

$$\hat{\boldsymbol{\sigma}}^{\log} = \mathscr{L} : \mathbf{D}^{\text{e}} = \mathscr{L} : (\mathbf{D} - \mathbf{D}^{\text{in}}) = \mathscr{L} : \mathbf{D} - \sqrt{6}\mu\overline{D}^{\text{in}}\mathbf{n} \tag{5}$$

where μ is the shear modulus.

The evolution equation for the deviatoric part of Cauchy stress can be written as

$$\hat{\mathbf{s}}^{\log} = 2\mu(\mathbf{d} - \mathbf{d}^{\text{in}}) = 2\mu\mathbf{d} - \sqrt{6}\mu\overline{D}^{\text{in}}\mathbf{n} \tag{6}$$

The evolution equation for the equilibrium stress deviator is assumed to be of the form (Krempl, 1996)

$$\hat{\mathbf{g}}^{\log} = \frac{\psi}{E}\left(\hat{\mathbf{s}}^{\log} + \frac{\mathbf{o}}{\kappa(\Gamma)} - \frac{\Gamma}{\kappa(\Gamma)}\frac{(\mathbf{g}-\mathbf{f})}{A}\right) + \left(1 - \frac{\psi}{E}\right)\hat{\mathbf{f}}^{\log} \tag{7}$$

E is Young's modulus and the positive, decreasing shape function, ψ, controls the transition from the initial quasi-elastic behavior and the fully established inelastic flow. The kinematic stress, $\mathbf{f}$ is a tensorial state variable of FVBO introduced to model the monotonic work hardening. A is the rate-independent isotropic stress, a scalar state variable of FVBO. The evolution equation of the kinematic stress, $\mathbf{f}$, is taken as

$$\hat{\mathbf{f}}^{\log} = \overline{E}_{\text{t}}\mathbf{d}^{\text{in}} \tag{8}$$

$$\overline{E}_{\text{t}} = \frac{2}{3}\frac{E_{\text{t}}}{\left(1 - \frac{E_{\text{t}}}{E}\right)}. \tag{9}$$

E_{t} is the terminating slope of the uniaxial stress/strain curve at maximum strain of interest.

The isotropic stress, A, could be assumed to evolve according to

$$\dot{A} = A_c(A_f - A)\overline{D}^{\text{in}} \tag{10}$$

with initial value

$$A(t=0) = A_0. \tag{11}$$

A_0, A_c and A_f are material constants. The evolution of the state variable A allows the modeling of cyclic hardening or softening behavior. We note that (8) has the same form as the Prager kinematic hardening law in rate-independent plasticity theory, hence **f** has been named the kinematic stress.

Following Yao and Krempl (1978) the material functions ψ and κ are given by

$$\psi(\Gamma) = a_1 + (a_2 - a_1)\exp(-a_3\Gamma) \tag{12}$$

and

$$\kappa(\Gamma) = b_1\left(1 + \frac{\Gamma}{b_2}\right)^{-b_3}. \tag{13}$$

In (12) and (13), a_1, a_2, a_3, b_1, b_2 and b_3 are material constants and they can be determined from experiments specified by Yao and Krempl (1978), Krempl and Yao (1987), Maciucescu et al. (1999) and Tachibana and Krempl (1998).

The positive, decreasing, nonzero viscosity function $\kappa[\Gamma]$ was adopted from viscoelasticity theory. In viscoplasticity the flow function $F[\frac{\Gamma}{\Delta}]$ and the scalar drag stress Δ, are well known. The relation between F and κ functions can be obtained from Eq. (3) to yield $\overline{D}^{\text{in}} = \Gamma/E\kappa[\frac{\Gamma}{\Delta}] = F[\frac{\Gamma}{\Delta}]$. It is deduced that the flow function $F[\frac{\Gamma}{\Delta}]$ is positive, increasing and that $F[0] = 0$. The frequently used power law satisfies these conditions. The two approaches are equivalent. These modifications are used by Tachibana and Krempl (1998) to reduce the number of constants from 18 to 10. It was proposed by Maciucescu et al. (1999) who modeled monotonic and cyclic motions of solder with good success.

After studying the set of equations and the role of the shape function ψ Majors and Krempl (1994a) suggested to employ two separate shape functions $\bar{\psi}_1$ and $\bar{\psi}$ so that

$$\hat{\mathbf{g}}^{\log} = \bar{\psi}_1\hat{\mathbf{s}}^{\log} + F[\Gamma/\Delta]E\bar{\psi}\left(\frac{\mathbf{o}}{\Gamma} - \frac{\mathbf{g}-\mathbf{f}}{A+\beta\Gamma}\right) + (1-\bar{\psi}_1)\hat{\mathbf{f}}^{\log} \tag{14}$$

The functions are limited by $0 \leqslant \bar{\psi}_1 < 1$ and $\bar{\psi} > 0$. They can be functions of the overstress or can be constants. We have recently used two shape constants, $\bar{\psi}_1$ and $\bar{\psi}$ with success. This split-up was sufficient for our modeling needs. If $\bar{\psi}_1 = 0$, elastic hardening cannot be modeled. The quantity $\bar{\psi} > 0$ affects the transition from quasi-elastic behavior to the established flow stress region where the tangent modulus is small compared to the elastic modulus.

Further constitutive equations are reported by Ho and Krempl (2001a) and include formulations that model inelastic compressibility. The dimensionless factor β in Eq. (16) of Ho and Krempl (2001a,b,c) is zero for "normal" VBO that models positive rate sensitivity. Setting $\beta < -1$, $\beta = -1$, $\beta \geqslant -1$ produces negative, zero and positive rate sensitivity, respectively. Details can be found in Ho and Krempl (2000, 2001b,c).

The isotropic, finite viscoplasticity continuum model is experiment based and is able to represent nonlinear creep, relaxation and nonlinear loading rate sensitivity (see Tachibana and Krempl, 1998; Maciucescu et al., 1999; Majors and Krempl, 1994b; Ho and Krempl, 2000, 2001a,b,c).

In addition, the model can be applied to cyclic loading. The inelastic incompressible constitutive equation consists of the flow law in two forms. In Eq. (3) the stress is the independent variable; its easily inverted form is found in Eq. (5). Aside from two elastic constants the flow law contains the overstress (**o**) and the scalar flow function F, as well as the scalar valued drag stress Δ. The Cauchy stress deviator tensor

and the equilibrium stress deviator (**g**) control the inelastic flow through the overstress (**o**), which is the difference $\mathbf{s}-\mathbf{g}$. The growth of the equilibrium stress is affected by the growth of the scalar isotropic stress (A) and by the growth of the drag stress (Δ). The isotropic and drag stress must always be positive. The FVBO model with constant isotropic and drag stresses produces, for a constant loading rate, responses akin to isotropic/kinematic hardening in plasticity. The isotropic stress has the same function in plasticity as in FVBO. It models the cyclic hardening or softening according to the postulated growth of A. FVBO can also represent nonlinear creep, relaxation and rate sensitivity. In FVBO there are no yield surfaces no loading/unloading conditions. There are no exactly linear elastic regions, only points at which the slope is equal to the elastic modulus, then $\mathbf{s}-\mathbf{g}=0$, which implies that either $\mathbf{s}\neq 0$ and $\mathbf{s}-\mathbf{g}=0$ or $\mathbf{s}=\mathbf{g}=0$. The model is competent to reproduce quasi-linear elastic regions, such as the unloading/reloading curves in the simulation of uniaxial tests, see Krempl (1996), Figs. 7 and 8 and Figs. 11 and 12. While there is no strain measure apparent, the integration of the rate of deformation using the unique logarithmic spin results in the Hencky strain $\ln\mathbf{V}$, which together with the Cauchy stress forms a work conjugate pair (Xiao et al., 1997).

3. Integration of constitutive equations

Within the context of displacement based finite element formulation, the time integration of the constitutive equations for a material point can be cast as an initial value problem.

Denoting the time at the beginning of the increment by t_n and the time at the end of the increment by t_{n+1}, given the value of $\boldsymbol{\sigma},\mathbf{g},\mathbf{f},A,\mathbf{d}^{\text{in}}$ at the time t_n, and $\mathbf{D}$ at time t_{n+1}, determine the values of $\boldsymbol{\sigma},\mathbf{g},\mathbf{f},A,\mathbf{d}^{\text{in}}$ at the time t_{n+1}.

The procedure of Reed and Atluri (1983) is used to enforce the incremental objectivity of the integration scheme. The integration of (4), for Cauchy stress, results in (Reed and Atluri, 1983)

$$\boldsymbol{\sigma}_{n+1}=\mathbf{Q}_{n+1}\boldsymbol{\sigma}_n\mathbf{Q}_{n+1}^{\mathrm{T}}+\mathbf{Q}_{n+1}\left(\int_{t_n}^{t_{n+1}}\mathbf{Q}(\xi)^{\mathrm{T}}\hat{\boldsymbol{\sigma}}^{\log}(\xi)\mathbf{Q}(\xi)\mathrm{d}\xi\right)\mathbf{Q}_{n+1}^{\mathrm{T}}. \tag{15}$$

The objective, generalized midpoint rule for (15) can be written as

$$\boldsymbol{\sigma}_{n+1}=\mathbf{Q}_{n+1}\boldsymbol{\sigma}_n\mathbf{Q}_{n+1}^{\mathrm{T}}+\Delta t\mathbf{Q}_{n+1}\mathbf{Q}_{n+\theta}^{\mathrm{T}}\hat{\boldsymbol{\sigma}}_{n+\theta}^{\log}\mathbf{Q}_{n+\theta}\mathbf{Q}_{n+1}^{\mathrm{T}} \tag{16}$$

where $\mathbf{Q}_{n+1}$ is given by

$$\mathbf{Q}_{n+1}=\exp(\Delta t\boldsymbol{\Omega}^*) \tag{17}$$

and

$$\boldsymbol{\Omega}^*=\boldsymbol{\Omega}^{\log}\left(t_{n+\frac{1}{2}}\right) \tag{18}$$

The tensor function $\exp(\Delta t\boldsymbol{\Omega}^*)$ has the representation (Schwerdtfeger, 1961)

$$\exp(\boldsymbol{\Omega}^*\Delta t)=\mathbf{I}+(\sin\omega\Delta t)\overline{\boldsymbol{\Omega}}+(1-\cos\omega\Delta t)\bar{\boldsymbol{\Omega}}^2 \tag{19}$$

where the normalized tensor $\bar{\boldsymbol{\Omega}}$ is given by

$$\overline{\boldsymbol{\Omega}}=\frac{\boldsymbol{\Omega}^*}{\omega} \tag{20}$$

and

$$\omega^2=(\boldsymbol{\Omega}_{12}^*)^2+(\boldsymbol{\Omega}_{13}^*)^2+(\boldsymbol{\Omega}_{23}^*)^2. \tag{21}$$

3.1. Explicit integration scheme

Following Sham and Chow (1999), a one-step forward gradient method will be used for integrating the material response. For generally good accuracy, θ in (16) is set to $\frac{1}{2}$ and (16) reduces to (Reed and Atluri, 1983)

$$\boldsymbol{\sigma}_{n+1} = \bar{\boldsymbol{\sigma}} + \Delta t \mathbf{H} \hat{\boldsymbol{\sigma}}^{\log}_{n+\frac{1}{2}} \mathbf{H}^{\mathrm{T}} \tag{22}$$

where

$$\mathbf{H} = (\mathbf{Q}_{n+1})^{1/2} \tag{23}$$

and

$$\bar{\boldsymbol{\sigma}} = \mathbf{Q}_{n+1} \boldsymbol{\sigma}_n (\mathbf{Q}_{n+1})^{\mathrm{T}}. \tag{24}$$

A similar expressions for the equilibrium stress and kinematic stress can be obtained as

$$\mathbf{g}_{n+1} = \bar{\mathbf{g}}_n + \Delta t \mathbf{H} \hat{\mathbf{g}}^{\log}_{n+\frac{1}{2}} \mathbf{H}^{\mathrm{T}} \tag{25}$$

$$\mathbf{f}_{n+1} = \bar{\mathbf{f}}_n + \Delta t \mathbf{H} \hat{\mathbf{f}}^{\log}_{n+\frac{1}{2}} \mathbf{H}^{\mathrm{T}} \tag{26}$$

where

$$\bar{\mathbf{g}}_n = \mathbf{Q}_{n+1} \mathbf{g}_n (\mathbf{Q}_{n+1})^{\mathrm{T}} \tag{27}$$

$$\bar{\mathbf{f}}_n = \mathbf{Q}_{n+1} \mathbf{f}_n (\mathbf{Q}_{n+1})^{\mathrm{T}}. \tag{28}$$

Let $\Delta \bar{e}^{\mathrm{in}}$ be the increment of the accumulated inelastic equivalent strain, i.e.

$$\Delta \bar{e}^{\mathrm{in}} = \bar{e}^{\mathrm{in}}_{n+1} - \bar{e}^{\mathrm{in}}_n. \tag{29}$$

Employing a linear interpolation in time to approximate $\Delta \bar{e}^{\mathrm{in}}$, one gets

$$\Delta \bar{e}^{\mathrm{in}} = \Delta t \left((1-\eta) \overline{D}^{\mathrm{in}}_n + \eta \overline{D}^{\mathrm{in}}_{n+1} \right), \tag{30}$$

where

$$0 \leqslant \eta \leqslant 1. \tag{31}$$

For $\eta = 0$, (30) reduces to the explicit Euler formula. For other values of η in the above range, (30) represent an implicit scheme since $\overline{D}^{\mathrm{in}}_{n+1}$ is not known a priori and an iterative algorithm is required.

The details can be found in Gomaa (2000). Box 1 describes the steps employed. The expressions for the one-step integration formula are

$$\hat{\mathbf{s}}^{\log} = 2\mu \mathcal{Q}^{\tan}_{\mathrm{s}} : \mathbf{d} - 2\mu\zeta \mathbf{n} \tag{32}$$

$$\hat{\mathbf{f}}^{\log} = \overline{E}_{\mathrm{t}} \mathcal{Q} : \mathbf{d} + \overline{E}_{\mathrm{t}} \zeta \mathbf{n} \tag{33}$$

$$\hat{\mathbf{g}}^{\log} = \frac{\psi}{E} \hat{\mathbf{s}}^{\log} + \left(1 - \frac{\psi}{E}\right) \hat{\mathbf{f}}^{\log} + \sqrt{\frac{2}{3}} \psi (\alpha(\mathbf{n} : \mathbf{d}) + \zeta) \left(\sqrt{\frac{2}{3}} \mathbf{n} + \frac{(\mathbf{g} - \mathbf{f})}{A} \right). \tag{34}$$

Box 1. Algorithm for the explicit integration scheme

(i) Given incr. displ. $\Delta\mathbf{u}$, calculate $\Delta t\mathbf{D}$ and update $\mathbf{F}$

$$\Delta t\mathbf{D}_{n+\frac{1}{2}} := \operatorname{sym}\left(\frac{\partial \Delta\mathbf{u}_{n+1}}{\partial \mathbf{x}_{n+\frac{1}{2}}}\right)$$

$$\mathbf{d}_{n+\frac{1}{2}} := \mathbf{D}_{n+\frac{1}{2}} - \frac{1}{3}(\mathbf{D}_{n+\frac{1}{2}} : \mathbf{I})\mathbf{I}$$

$$\mathbf{F}_r := \mathbf{I} + \frac{\partial \Delta\mathbf{u}_{n+1}}{\partial \mathbf{x}_n}$$

$$\mathbf{F}_{n+1} := \mathbf{F}_r\mathbf{F}_n$$

(ii) Compute the rotation tensor $\mathbf{Q}_{n+1}$ and rotate the state forward

$$\bar{\boldsymbol{\sigma}}_n := \mathbf{Q}_{n+1}\boldsymbol{\sigma}_n(\mathbf{Q}_{n+1})^{\mathrm{T}}$$

$$\bar{\mathbf{g}}_n := \mathbf{Q}_{n+1}\mathbf{g}_n(\mathbf{Q}_{n+1})^{\mathrm{T}}$$

$$\bar{\mathbf{f}}_n := \mathbf{Q}_{n+1}\mathbf{f}_n(\mathbf{Q}_{n+1})^{\mathrm{T}}$$

(iii) Compute the overstress, Γ and $\mathbf{n}$

$$\bar{\mathbf{s}}_n := \bar{\boldsymbol{\sigma}}_n - \frac{1}{3}(\bar{\boldsymbol{\sigma}}_n : \mathbf{I})\mathbf{I}$$

$$\mathbf{o}_n := \bar{\mathbf{s}} - \bar{\mathbf{g}}$$

$$\Gamma_n := \sqrt{\frac{3}{2}\mathbf{o}_n : \mathbf{o}_n}$$

$$\mathbf{n}_n := \sqrt{\frac{3}{2}}\frac{\mathbf{o}_n}{\Gamma_n}$$

(iv) Compute $\mathscr{Q}$, $\mathscr{Q}_{\mathrm{s}}^{\tan}$ and $\mathbf{D}^{\mathrm{in}}$

$$\mathscr{Q} := \alpha_n\mathbf{n}_n \otimes \mathbf{n}_n$$

$$\mathscr{Q}_{\mathrm{s}}^{\tan} := \mathscr{I} - \mathscr{Q}$$

$$\mathbf{D}^{\mathrm{in}} := \mathscr{Q}\mathbf{d}_{n+\frac{1}{2}} + \zeta\mathbf{n}_n$$

(v) Compute $\hat{\boldsymbol{\sigma}}^{\log}$, $\hat{\mathbf{f}}^{\log}$ and $\hat{\mathbf{g}}^{\log}$

$$\hat{\boldsymbol{\sigma}}^{\log} := \mathscr{L} : \mathbf{D}_{n+\frac{1}{2}} - 2\mu\zeta\mathbf{n}_n$$

$$\hat{\mathbf{f}}^{\log} := \overline{E}_{\mathrm{t}}\mathscr{Q} : \mathbf{d}_{n+\frac{1}{2}} + \overline{E}_{\mathrm{t}}\zeta\mathbf{n}_n$$

$$\hat{\mathbf{g}}^{\log} := \frac{\psi}{E}\hat{\mathbf{s}}^{\log} + \left(1 - \frac{\psi}{E}\right)\hat{\mathbf{f}}^{\log} + \sqrt{\frac{2}{3}}\psi_n(\alpha_n(\mathbf{n}_n : \mathbf{d}_{n+\frac{1}{2}}) + \zeta_n)\left(\sqrt{\frac{2}{3}}\mathbf{n}_n + \frac{(\bar{\mathbf{g}}_n - \bar{\mathbf{f}}_n)}{A_n}\right)$$

(vi) Update the stress and the internal variables

$$\boldsymbol{\sigma}_{n+1} := \bar{\boldsymbol{\sigma}}_n + \Delta t\hat{\boldsymbol{\sigma}}^{\log}$$

$$\mathbf{f}_{n+1} := \bar{\mathbf{f}}_n + \Delta t\hat{\mathbf{f}}^{\log}$$

$$\mathbf{g}_{n+1} := \bar{\mathbf{g}}_n + \Delta t\hat{\mathbf{g}}^{\log}$$

$$A_{n+1} := A_c(A_f - A_n)\overline{D}_n^{\mathrm{in}}$$

The symmetric fourth-order tensor $\mathscr{Q}_{\mathrm{s}}^{\tan}$ is given by

$$\mathscr{Q}_{\mathrm{s}}^{\tan} = \mathscr{I} - \mathscr{Q}. \tag{35}$$

The fourth-order tensor $\mathscr{Q}$ is defined as

$$\mathscr{Q} = \alpha \mathbf{n} \otimes \mathbf{n} \tag{36}$$

where

$$\alpha = \sqrt{\frac{3}{2}} \Delta t P \frac{\eta}{\xi} \frac{\mathrm{d}C}{\mathrm{d}\Gamma} \tag{37}$$

and $\mathscr{I}$ is the fourth-order, symmetric identity tensor. Cauchy stress, equilibrium stress and kinematic stress can be updated using (22), (25) and (26). One notes, however, that all tensors are evaluated at time t_n except the rate of deformation tensor $\mathbf{D}$, which is evaluated at $t_{n+\frac{1}{2}}$.

3.1.1. Material Jacobian matrix

In this section the material Jacobian matrix required for the finite element formulation, consistent with the integration algorithm obtained in the previous section, will be derived.

Eq. (22) can be written as

$$\boldsymbol{\sigma}_{n+1} = \bar{\boldsymbol{\sigma}} + \Delta \boldsymbol{\sigma}_{n+1}. \tag{38}$$

Using (32), $\Delta \boldsymbol{\sigma}_{n+1}$ can be approximated by

$$\Delta \boldsymbol{\sigma}_{n+1} = 2\mu \mathscr{Q}_{\mathrm{s}}^{\tan} : \left(\Delta \boldsymbol{\epsilon} - \frac{1}{3} (\Delta \boldsymbol{\epsilon} : \mathbf{I}) \mathbf{I} \right) + K (\Delta \boldsymbol{\epsilon} : \mathbf{I}) \mathbf{I} - 2\mu \zeta \mathbf{n} \tag{39}$$

where K is the bulk modulus, $\mathbf{I}$ is the second-order identity tensor and $\Delta \boldsymbol{\epsilon}$ is given by

$$\Delta \boldsymbol{\epsilon} = \Delta t \mathbf{D}. \tag{40}$$

Only the operator $\frac{\partial \Delta \boldsymbol{\sigma}_{n+1}}{\partial \Delta \boldsymbol{\epsilon}}$ will be considered here. For simplicity the subscript $n+1$ is dropped. Taking the partial derivative of (39) with respect to $\Delta \boldsymbol{\epsilon}$, results in the material Jacobian matrix

$$\frac{\partial \Delta \boldsymbol{\sigma}}{\partial \Delta \boldsymbol{\epsilon}} = 2\mu \mathscr{Q}_{\mathrm{s}}^{\tan} - \left(\frac{2\mu}{3} - K \right) \mathbf{I} \otimes \mathbf{I}. \tag{41}$$

3.2. Implicit integration scheme

In this section, the backward Euler method will be used to integrate the FVBO constitutive equations. The integration algorithm is similar to that developed by Sham (1994) for infinitesimal strain, thermal VBO. The equations is written at the time t_{n+1} and the backward Euler method will be used to integrate the rates. For backward Euler method, θ is set to 1 in (16) and it reduces to

$$\boldsymbol{\sigma}_{n+1} = \bar{\boldsymbol{\sigma}} + \Delta t (\hat{\boldsymbol{\sigma}}^{\log})_{n+1} \tag{42}$$

where

$$\bar{\boldsymbol{\sigma}} = \mathbf{Q}_{n+1} \boldsymbol{\sigma}_n \mathbf{Q}_{n+1}^{\mathrm{T}}. \tag{43}$$

As in the explicit case the details are omitted, but Box 2 lists the necessary steps. Details are found in Gomaa (2000).

Box 2. Algorithm for the implicit integration scheme

(i) Given incr. displ. $\Delta\mathbf{u}$, calculate $\Delta t\mathbf{D}$ and update $\mathbf{F}$

$$\Delta t\mathbf{D}_{n+1} := \operatorname{sym}\left(\frac{\partial \Delta\mathbf{u}_{n+1}}{\partial \mathbf{x}_{n+1}}\right)$$

$$\mathbf{d}_{n+1} := \mathbf{D}_{n+1} - \frac{1}{3}(\mathbf{D}_{n+1} : \mathbf{I})\mathbf{I}$$

$$\mathbf{F}_r := \mathbf{I} + \frac{\partial \Delta\mathbf{u}_{n+1}}{\partial \mathbf{x}_n}$$

$$\mathbf{F}_{n+1} := \mathbf{F}_r\mathbf{F}_n$$

(ii) Compute the rotation tensor $\mathbf{Q}_{n+1}$ and rotate the state forward

$$\bar{\boldsymbol{\sigma}}_n := \mathbf{Q}_{n+1}\boldsymbol{\sigma}_n(\mathbf{Q}_{n+1})^{\mathrm{T}}$$

$$\bar{\mathbf{g}}_n := \mathbf{Q}_{n+1}\mathbf{g}_n(\mathbf{Q}_{n+1})^{\mathrm{T}}$$

$$\bar{\mathbf{f}}_n := \mathbf{Q}_{n+1}\mathbf{f}_n(\mathbf{Q}_{n+1})^{\mathrm{T}}$$

(iii) Solve the nonlinear equation $F(\Gamma_{n+1}) = 0$ for Γ_{n+1}

(iv) Compute $\overline{D}^{\mathrm{in}}_{n+1}$, $\mathbf{D}^{\mathrm{in}}_{n+1}$ and $\mathbf{n}_{n+1}$

$$\overline{D}^{\mathrm{in}}_{n+1} := \frac{\Gamma_{n+1}}{E\kappa_{n+1}}$$

$$\mathbf{D}^{\mathrm{in}}_{n+1} := \frac{3}{2}\overline{D}^{\mathrm{in}}_{n+1}\frac{\mathbf{O}_{n+1}}{\Gamma_{n+1}}$$

$$\mathbf{n}_{n+1} := \sqrt{\frac{3}{2}}\frac{\mathbf{O}_{n+1}}{\Gamma_{n+1}}$$

(v) Update the stress and the internal variables

$$\boldsymbol{\sigma}_{n+1} := \boldsymbol{\sigma}^* - \sqrt{6}\mu\Delta t\overline{D}^{\mathrm{in}}_{n+1}\mathbf{n}_{n+1}$$

$$\mathbf{g}_{n+1} := \frac{1}{C_1}(\mathbf{g}^* + C_2\mathbf{n}_{n+1})$$

$$\mathbf{f}_{n+1} := \bar{\mathbf{f}}_n + \sqrt{\frac{3}{2}}\overline{E}_{\mathrm{t}}\Delta t\mathbf{n}_{n+1}$$

The material Jacobian matrix has been derived. It is required for the finite element formulation, consistent with the implicit integration algorithm obtained in the previous section (Gomaa, 2000). It is noted that the formulation of the material Jacobian matrix does not affect the accuracy of the solution; however, an operator that is consistent with the integration algorithm is essential to maintain the quadratic rate of convergence of the iterative method used to solve the nonlinear finite element equations (Simo and Hughes, 1998).

The Jacobian matrix is given in Gomaa (2000) and is not cited here for the sake of brevity.

4. Numerical examples

The isotropic FVBO theory has been implemented as a material subroutine (UMAT) in the commercial finite element program ABAQUS (HKS, 1995) Both the forward gradient and the implicit

Table 1
Material constants for FVBO

Constant	Value
E	1.95E5 MPa
v	0.30
E_t	5.00E2 MPa
A_c	10
A_f	2.15E2 MPa
A_0	1.15E2 MPa
a_1	7.90E4 MPa
a_2	1.83E5 MPa
a_3	0.08 $(\text{MPa})^{-1}$
b_1	3.14E5 s
b_2	60.00 MPa
b_3	21.98

integration schemes are available. The material subroutine has been used, within ABAQUS, to solve some boundary value problems. Table 1 summarizes the material properties used for all the numerical experiments.

4.1. Comparison with ODE solution and the influence of step size

In these series of calculations, the finite element solution based on one element is compared with the numerical solution as obtained from the ordinary differential equation solver LSODA (Hindmarsh, 1983).

The first comparison is for the case of plane strain axial tension. A constant engineering strain rate, $\dot{\varepsilon} = 10^{-4}/s$, was imposed and the finite element solution was obtained using both the forward gradient and the implicit integration methods. For the forward gradient method, several time step sizes $\frac{\Delta t}{t_0} = 0.5$, $\frac{\Delta t}{t_0} = 0.2$ and $\frac{\Delta t}{t_0} = 0.1$ were tried and for the implicit integration scheme a uniform time step of $\frac{\Delta t}{t_0} = 10$ was used. The reference time t_0 is taken as $\frac{\sigma_0}{E\dot{\varepsilon}}$, where σ_0 is the yield stress in tension.

The true stress versus the logarithm of the stretch λ (the true strain) curves for both the forward gradient finite element and the ODE solutions are shown in Fig. 1. Fig. 2 shows the implicit finite element and the ODE solutions. As seen from the figures, the forward gradient integration scheme requires very small time

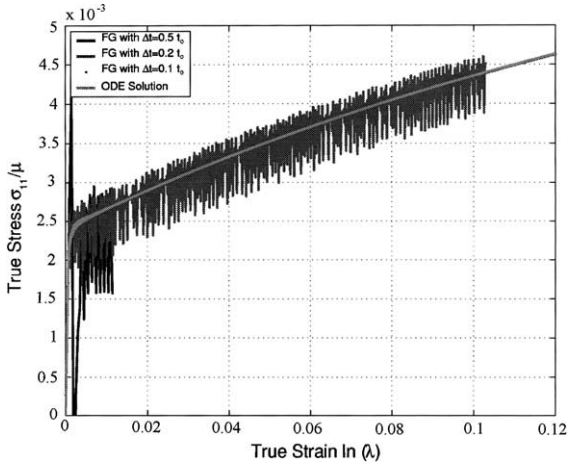

Fig. 1. Comparison between the results from the ordinary differential equation solver LSODA and the forward gradient, finite element solutions with different step sizes for the case of uniaxial tension.

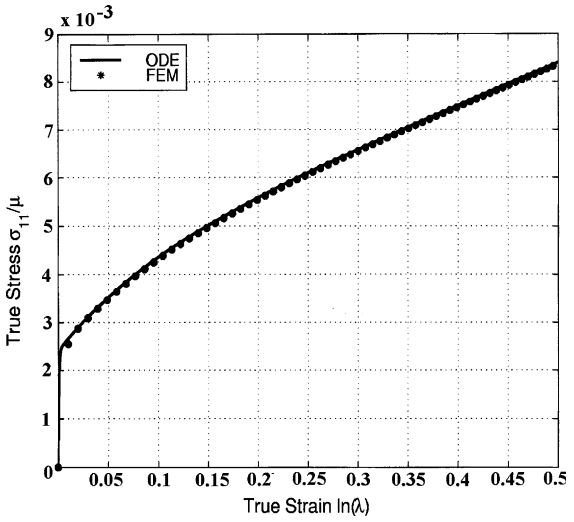

Fig. 2. Comparison between the results from the ordinary differential equation solver LSODA and the implicit backward Euler finite element solutions for the case of uniaxial tension.

steps, however, the implicit integration gives good agreement with the ODE solution using a time step that is hundred times larger than the steps recorded for the forward gradient integration. This, clearly, shows the advantage of the implicit integration over the forward gradient integration scheme.

The second comparison is for the case of simple shear. The finite element solution was obtained using the implicit integration method with uniform time step size $\frac{\Delta t}{t_0} = 16$. The true stress versus the nominal shear strain curves for both the finite element and ODE solutions are shown in Figs. 3 and 4. As seen from the figures, the finite element solutions compare well with the ODE solutions. The finite element solution coincides with the ODE solution in the limit even when the time step size $\frac{\Delta t}{t_0}$ becomes very small.

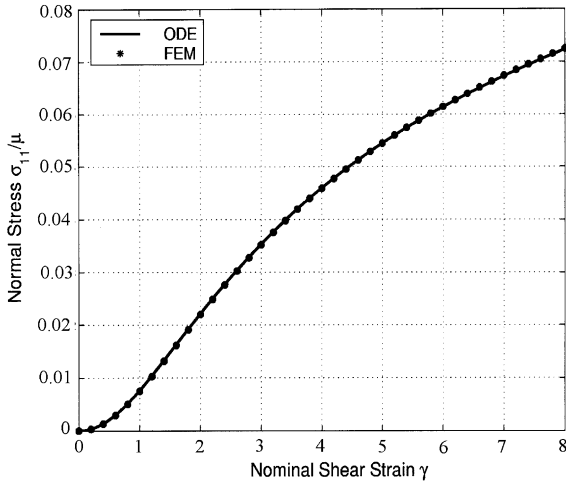

Fig. 3. Comparison between the results from the ordinary differential equation solver LSODA and the backward Euler finite element solutions for the case of simple shear.

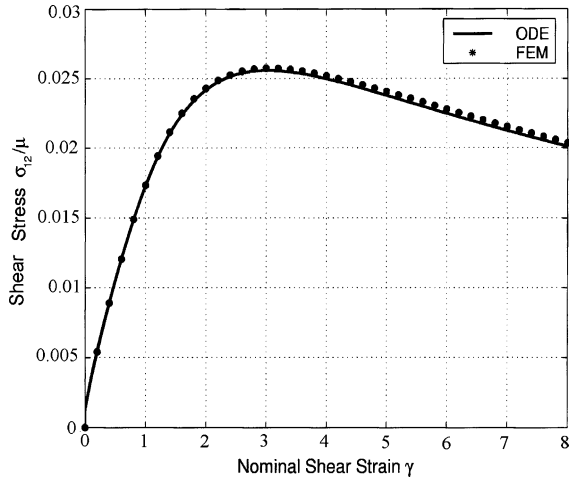

Fig. 4. Comparison between the ordinary differential equation solver LSODA and the backward Euler finite element solutions for the case of simple shear.

4.2. Strain rate sensitivity

To demonstrate the capability of the finite element formulation to capture the strain rate sensitivity, a plane strain finite element model was subjected to the following strain-rate history. The strain rate was kept at $\dot{\varepsilon} = 10^{-5}/s$ then increased to $\dot{\varepsilon} = 10^{-1}/s$ and finally returned back to $\dot{\varepsilon} = 10^{-5}/s$.

Fig. 5 shows the true stress plotted versus the logarithm of the stretch λ (the true strain) for this case. Note, the stretch is continuous upon a jump in strain rate. The yield-point-like overshoots/undershoots are a part of the (FVBO) predictions and can be affected by changing the constant a_3 in Eq. (12) or equivalently in Eq. (14). The figure shows that the strain rate sensitivity is captured. No strain rate history effect is modeled.

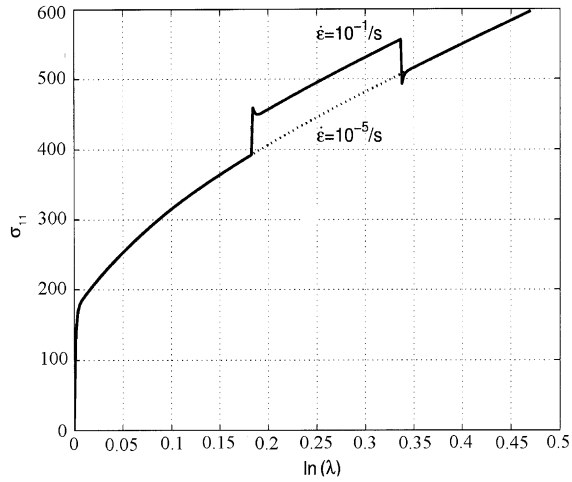

Fig. 5. Axial tension; strain rate sensitivity.

4.3. Axial cyclic loading

A plane strain finite element was subjected to uniaxial cyclic loading with strain control to simulate the cyclic effect. The true-strain rate alternated between $\pm 10^{-4}$/s as the material was cycled in true-strain range $(-0.4, 0.4)$. One cycle was simulated. The graph of true-stress σ_{11} versus the true-strain $\ln(\lambda)$ is shown in Fig. 6. The sharp transition from the predominantly elastic to inelastic behavior is due to the scale. Note that the strain range is 0.8 and the chosen E_t is comparatively large.

4.4. Simple shear

Figs. 7 and 8 show the stresses obtained for the simple shear problem using the Jaumann, the Green–Naghdi and the logarithmic rates. In contrast to the Jaumann rate, the logarithmic rate and the

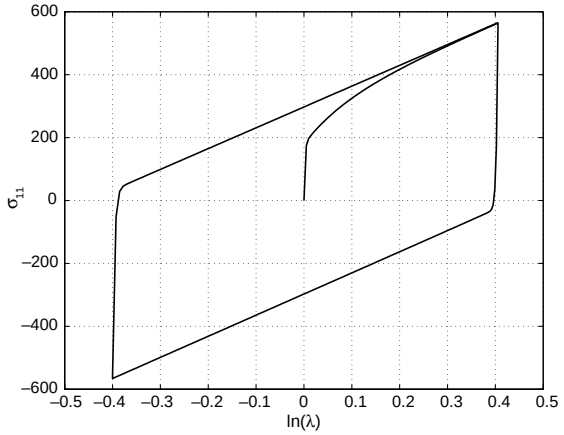

Fig. 6. Axial cyclic loading; σ_{11} versus $\ln(\lambda)$ for nominal strain rate $\dot{\varepsilon} = \pm 10^{-4}/s$.

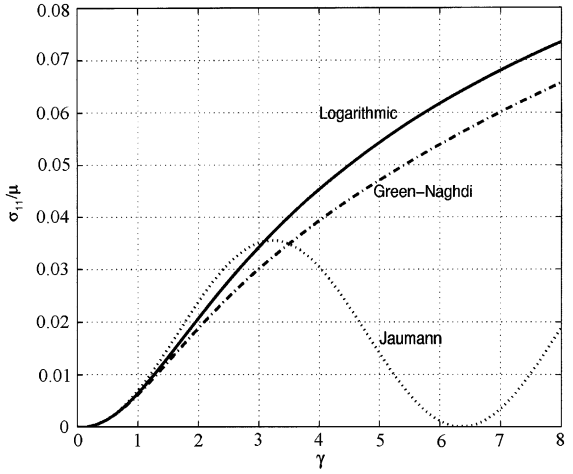

Fig. 7. Simple shear; normalized true stress σ_{11}/μ versus shear strain.

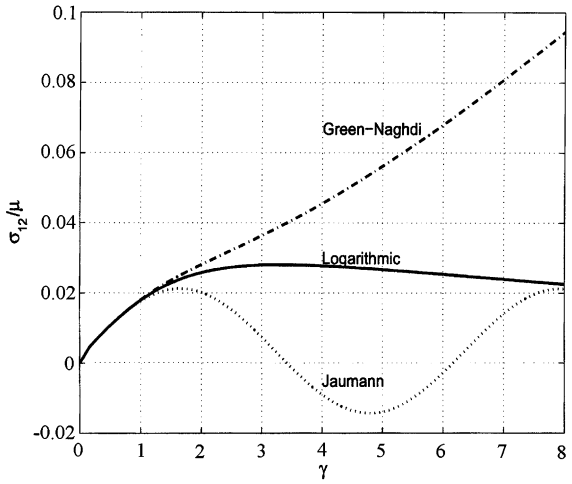

Fig. 8. Simple shear; normalized true stress σ_{12}/μ versus shear strain.

Green–Naghdi rate do not exhibit an oscillatory response. This is one of the desirable properties of the logarithmic rate.

4.5. Free-end torsion

The purpose of this example is to study the behavior of a hollow cylinder subjected to a free-end torsion to see if FVBO can simulate the behavior observed by Swift (1947).

A hollow cylinder with 1.0 in. outside diameter, 0.9 in. inside diameter and 1 in. in length is meshed using 8-noded hexahedral 3D elements. A prescribed rotation is applied to the top nodes of the finite element mesh and equal and opposite rotation is applied to the bottom ones. The applied rotation is reversed to simulate torque reversal.

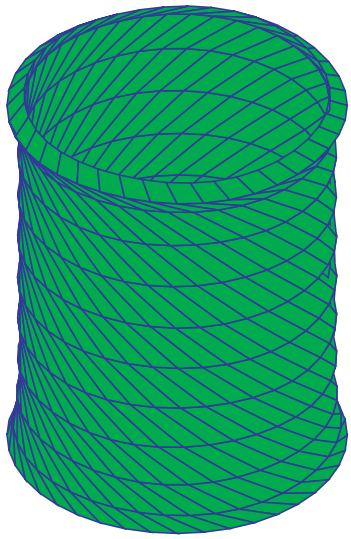

Fig. 9. Free-end torsion; deformed mesh for the case with a plug. Maximum shear strain $\gamma = 3.0$.

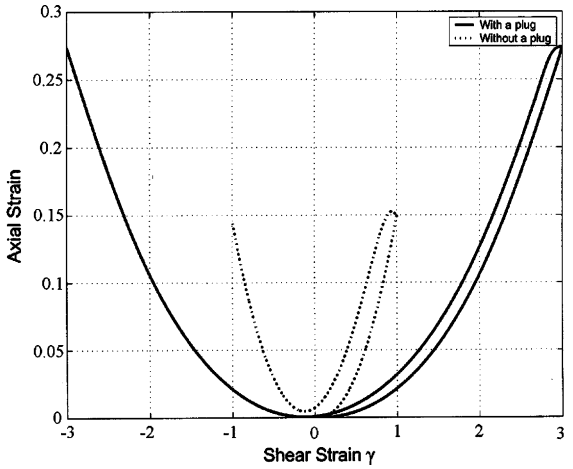

Fig. 10. Free-end torsion; axial strain versus shear strain for the cases with and without a plug.

At about shear strain equal to 1.0 the cylinder became highly distorted. To suppress these distortions a rigid cylinder is added to the model to simulate a rigid plug. The inside nodes of the hollow cylinder are allowed to slide along the surface of this plug without penetrating it. Fig. 9 depicts the deformed mesh after the plug had been used.

Fig. 10 shows the graphs of the unplugged and plugged cases together. It is seen that for both tests the unloading branch almost coincides with the loading branch but there is no cusp at the reversal points, which is seen in real experiments by Swift (1947).

As seen from the figures, the "backtracking" of the shear strain versus axial strain curves at torque reversals seen in experiments (Swift, 1947), is not modeled. This result is expected (see Majors and Krempl, 1994a,b), since the modeling of "backtracking" requires repository for texture induced anisotropy. It cannot be reproduced quantitatively by isotropic formulations using a backstress and appropriate spins alone. These observations would suggest that the developing of texture causes a change in anisotropy, which must be accounted for the modeling the "backtracking" (see Majors and Krempl, 1994b; Boehlke, 2001; Boehlke et al., 2003; Colak, 2001).

5. Discussion

5.1. Simple shear numerical experiments

The backward Euler implicit time integration scheme is shown to be efficient for the isotropic FVBO. The resulting stress–strain curves are smooth and free of oscillations and compare favorably with the curves obtained from ODE solver LSODA (Hindmarsh, 1983). Use of the forward gradient method resulted in oscillatory behavior at time steps about 100 times smaller than used in the implicit scheme, see Fig. 1.

When the FVBO theory was used to determine its response to simple shear, no oscillations were observed for the newly developed objective logarithmic stress rate (see Xiao et al., 1997). The usual oscillatory behavior is found when the Jaumann rate is used, see Figs. 7 and 8. The co-rotational Green–Naghdi rate yields a tensile response close to that of the logarithmic rate. In the shear response the Green–Naghdi rate grows without bounds at shear strains larger than 1.5. It appears that the logarithmic rate yields non-oscillatory response in simple shear that remains bounded. The use of the rate of deformation, the logarithmic rate and the Hencky strain $\ln\mathbf{V}$ suggests itself.

It has been shown in Xiao et al. (1997) that the rate of deformation is equal to the logarithmic rate of Hencky strain, which is based on the left stretch tensor **V**. The Hencky strain is the only strain that has this property. In this work, it has been shown that the use of the objective logarithmic rate produces no oscillations in simple shear, thus avoiding the criticism leveled at the Jaumann rate. Using the logarithmic rate form of Hooke's law, Gomaa (2000) has demonstrated that no dissipation takes place when strained in a closed path, see Figs. 11 and 12. This result is preferable to the one obtained with the Jaumann rate which leads to dissipation (see Kojic and Bathe, 1987; Pinsky et al., 1983).

The above demonstrates that the fundamental objections against hypoelastic Eulerian approach are no longer true and that the logarithmic time derivative has eliminated the objectionable oscillations in simple shear found with other objective rates.

The modeling of the unloading behavior for the free-end torsion was not very successful. This result had been expected since the present formulation is isotropic only. Models which represent the deformation induced anisotropy exist and these models show the change in anisotropy and the change in axial length with reasonable accuracy (see Boehlke, 2001; Boehlke et al., 2003; Gomaa, 2000; Colak, 2001).

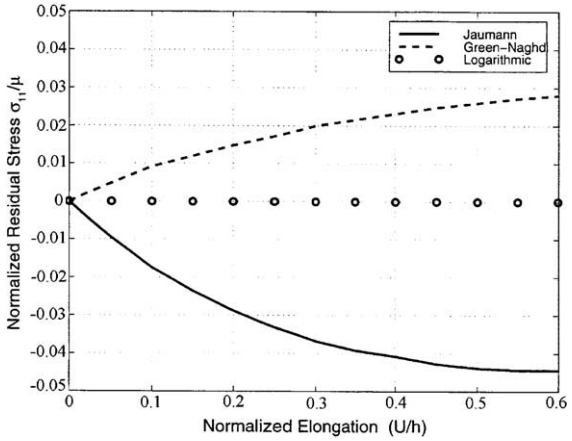

Fig. 11. Residual axial stresses versus normalized displacement in a closed elastic cycle.

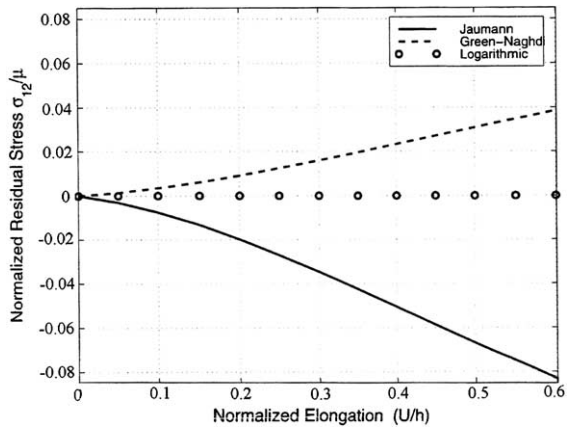

Fig. 12. Residual shear stresses versus normalized displacement in a closed elastic cycle.

5.2. The new method based on logarithmic rate

The use of the logarithmic rate has eliminated three objections that were leveled against the Eulerian method with the Jaumann rate (see Simo and Hughes, 1998, p.275). They are: "The hypoelastic nature of the stress response renders the model questionable on fundamental grounds, and limits its applicability to small elastic strains..." (Simo and Hughes, 1998, p. 275). It has been shown by Xiao et al. (1997), that using the co-rotational logarithmic rate, and the rate form of the isotropic Hooke's law involving the rate of deformation $\mathbf{D}$ and the Cauchy stress $\boldsymbol{\sigma}$, the relation $\mathbf{D} = \frac{1+v}{E}\hat{\boldsymbol{\sigma}}^{\log} - \frac{v}{E}(\mathrm{tr}\hat{\boldsymbol{\sigma}}^{\log})\mathbf{I}$ can be integrated to yield the finite hyperelastic law $\ln\mathbf{V} = \frac{1+v}{E}\boldsymbol{\sigma} - \frac{v}{E}(\mathrm{tr}\boldsymbol{\sigma})\mathbf{I}$, where E and v are the constant elastic modulus and Poisson's ratio, respectively (see Xiao et al., 1997; Bruhns et al., 1999). They demonstrate that an objective co-rotational rate of the Hencky strain $\ln\mathbf{V}$ is exactly identical with the rate of stretching. Of all strain measures only $\ln\mathbf{V}$ has this property.

"... limits its applicability to ... small elastic strains ..." (Simo and Hughes, 1998, p. 275). This property is not true for the isotropic rate form of Hooke's law cited above. No restriction on the magnitude of the Hencky strain $\ln\mathbf{V}$ exists any more.

"The choice of the kinematic hardening law has become a somewhat controversial issue because of results ..." (Simo and Hughes, 1998, p. 271). The results referred to are the oscillatory behavior in simple shear, which are shown not to occur for the logarithmic rate as demonstrated in Figs. 7 and 8.

Acknowledgements

Editorial assistance was provided by Dr. O. U. Colak.
The ABAQUS program is produced by ABAQUS, Inc. of Pawtucket RI.

References

Boehlke, T., 2001. Crystallographic texture evolution and elastic anisotropy: simulation, modeling,application. Ph.D. Thesis, Otto von Guericke Universitaet, Magdeburg, Magdeburg, Germany, February.

Boehlke, T., Bertram, A., Krempl, E., 2003. Modeling of deformation induced anisotropy in free-end torsion. International Journal of Plasticity 19, 1867–1885.

Bruhns, O.T., Xiao, H., Meyers, A., 1999. Self consistent Eulerian rate-type elasto-plasticity models based upon the logarithmic stress rate. International Journal of Plasticity 15, 479–520.

Colak, O., 2001. Modeling of proportional and non-proportional cyclic loading, ratcheting and deformation induced anisotropy using viscoplasticity theory based on overstress. Ph.D. Thesis, Rensselaer Polytechnic Institute, Troy, NY 12180.

Gomaa, S., 2000. Computational procedures for finite deformation rate-independent plasticity and viscoplasticity based on overstress. Ph.D. Thesis, Rensselaer Polytechnic Institute, Troy, NY.

Hindmarsh, A.C., 1983. ODEPACK, A systematized collection of ODE solvers. In: Stepleman, R. et al. (Eds.), Scientific Computing. IMACS/North-Holland Publishing Company, Amsterdam.

HKS, Inc., 1995. ABAQUS Theory Manual, Version 5.5. HKS, Inc., Rhode Island.

Ho, K., Krempl, E., 2000. Modeling of positive, negative and zero rate sensitivity by using the viscoplasticity theory based on overstress (VBO). Mechanics of Time-Dependent Materials 4, 21–42.

Ho, K., Krempl, E., 2001a. Inelastic compressible and incompressible, isotropic, small strain viscoplasticity theory based on overstress (VBO). In: Lemaitre, J. (Ed.), Lemaitre Handbook of Materials Behavior Models. Academic Press, New York, pp. 336–348 (Section 5.6).

Ho, K., Krempl, E., 2001b. Extention of the viscoplasticity theory based on overstress (VBO) to capture non-standard rate dependence in solids. International Journal of Plasticity 18, 851–872.

Ho, K., Krempl, E., 2001c. The modeling of unusual rate sensitivities inside and outside the dynamic strain aging regime. Journal of Engineering Materials and Technology 123, 28–35.

Kojic, M., Bathe, K.J., 1987. Studies of finite element procedures-stress solution of a closed elastic strain path with stretching and shearing using the updated Lagrangian Joumann formulation. Computers and Structures 26, 175–179.

Krempl, E., 1996. A Small-strain viscoplasticity theory based on overstress. In: Krausz, A., Krausz, K. (Eds.), Unified Constitutive Laws of Plastic Deformation. Academic Press, New York, pp. 281–318.

Krempl, E., Yao, D., 1987. Viscoplasticity theory based on overstress applied to ratchetting and cyclic hardening. In: Rie, K.T. (Ed.), Low Cycle Fatigue and ElastoPlastic Behavior of Materials. Elsevier Science, New York, pp. 137–148.

Maciucescu, L., Sham, T.-L., Krempl, E., 1999. Modeling the deformation behavior of an SN–PB solder alloy using the simplified viscoplasticity theory based on overstress (VBO). Journal of Electronic Packaging 121, 92–98.

Majors, P.S., Krempl, E., 1994a. The isotropic viscoplasticity theory based on overstress applied to the modeling of modified 9 wt.%Cr–1 wt.%Mo steel at 538 °C. Material Science and Engineering A 186, 23–34.

Majors, P.S., Krempl, E., 1994b. Comments on induced anisotropy, the Swift effect, and finite deformation inelasticity. Mechanical Communications, 21, 465–472.

Peirce, D., Shih, C.F., Needlman, A., 1984. A tangent modulus method for rate dependent solids. Computers and Structures 18, 875–887.

Pinsky, P., Ortiz, M., Pister, K.S., 1983. Numerical integration of rate constitutive equations in finite deformation analysis. Computer Methods in Applied Mechanics and Engineering 40, 137–158.

Reed, K.W., Atluri, S., 1983. Analysis of large quasistatic deformations of inelastic bodies by a new hybrid-stress finite element algorithm. Computer Methods Applied Mechanics and Engineering 39, 245–295.

Schwerdtfeger, H., 1961. Introduction to Linear Algebra and the Theory of Matrices. Groninger, P. Nordhoff.

Sham, T.-L., 1994. Implicit (backword Euler) integration method for a version of TVBO with constant isotropic stress and without static recovery. MML Report no l994-S2, Rensselaer Polytechnic Institute.

Sham, T.-L., Chow, H., 1999. A finite element method for incremental viscoplasticity theory based on overstress. European Journal of Mechanics A/Solids 8, 415–436.

Simo, J.C., Hughes, T., 1998. Computational Inelasticity. Springer-Verlag, New York.

Swift, H., 1947. Length changes in metals under torsional overstrain. Engineering 163, 253–257.

Tachibana, Y., Krempl, E., 1998. Modeling of high homologous temperature deformation behavior using the viscoplasticity theory based on overstress (VBO): part III—a simplified model. Journal of Engineering Materials and Technology 120, 193–196.

Xiao, H., Bruhns, O.T., Meyers, A., 1997. Logarithmic strain, logarithmic spin and logarithmic rate. Acta Mechanica 124, 89–105.

Yao, D., Krempl, E., 1978. Viscoplasticity theory based on overstress: the prediction of monotonic and cyclic proportional and nonproportional loadings paths for aluminum alloy. International Journal of Plasticity 1, 259–274.